Ecological Informatics 90 (2025) 103267

Contents lists available at ScienceDirect

Ecological Informatics

journal homepage: www.elsevier.com/locate/ecolinf

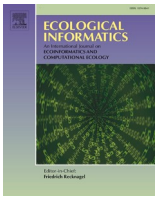

Distinguishing the main climatic drivers of terrestrial vegetation carbon dynamics in pan-Arctic ecosystems

Chengfeng Meng [a,b], Hao Zhou [a,b,*], Xichuan Liu [a,b], Jiao Zheng [c], Jun Wang [d], Qingwei Zeng [a,b], Shuai Hu [a,b]

[a] College of Meteorology and Oceanography, National University of Defense Technology, Changsha 410073, China
[b] Key Laboratory of High Impact Weather (Special), China Meteorological Administration (CMA), Changsha 410073, China
[c] Jiangsu Key Laboratory of Atmospheric Environment Monitoring and Pollution Control, Collaborative Innovation Center of Atmospheric Environment and Equipment Technology, School of Environmental Science and Engineering, Nanjing University of Information Science & Technology (NUIST), Nanjing 210044, China
[d] Frontiers Science Center for Critical Earth Material Cycling, International Institute for Earth System Science, Nanjing University, Nanjing 210023, China

ARTICLE INFO

Keywords:
Pan-Arctic
Vegetation index
Climate change
CO_2
VPD

ABSTRACT

Pan-Arctic terrestrial ecosystems have experienced widespread greening over the past few decades due to climate warming. However, the dynamic variations and climatic causes of such greening in the pan-Arctic are still unclear due to limitations in high-latitude ground-based measurements. The study first evaluated the applicability of three satellite-based vegetation indices (VIs) for pan-Arctic carbon dynamics in previous decades compared with multisource observations. Three VIs presented significant increasing trends up to 0.0005–0.0017 yr^{-1} for pan-Arctic ecosystems in the past 23 years, and near-infrared reflectance of vegetation (NIRv) could better capture pan-Arctic terrestrial carbon dynamic variations (e.g., increasing trends) than other VIs among most vegetation types, such as grasslands. The separate contributions of climatic factors to satellite-based NIRv variability were further quantified using partial correlation and ridge regression analysis over pan-Arctic ecosystems from 2001 to 2023. Carbon dioxide (CO_2) and air temperature (AT) presented positive partial correlations with the satellite-based NIRv over entire pan-Arctic ecosystems, due to fertilization and warming effects. However, the vapor pressure deficit (VPD) showed positive (negative) partial correlations with NIRv variations in high (low) pan-Arctic ecosystems because of diverse stomatal responses to air dryness. Therefore, increases in VPD contributed 11.2 % of the pan-Arctic NIRv variability, although positive (negative) effects were detected for high (low) pan-Arctic ecosystems. These findings highlight the advantages of the NIRv for representing terrestrial carbon dynamics in fragile ecosystems (e.g., the pan-Arctic) and reveal the diverse effects of the regional climate (e.g., air dryness) on pan-Arctic ecosystems under climate warming.

1. Introduction

Pan-Arctic terrestrial ecosystems play crucial roles in regulating global climate change and carbon cycles (Bruhwiler et al., 2021). As climatic amplifiers, pan-Arctic ecosystems present stronger warming responses to global carbon dioxide (CO_2) increases than low–middle latitudes did in several previous decades, leading to approximately three times greater temperature increases than the mean rates of global warming (Box et al., 2019). Elevated warming rates may enhance pan-Arctic terrestrial greening and carbon assimilation through modified vegetation dynamics, including extended growing season lengths (Myers-Smith et al., 2020) and increased vegetation species diversity (Thakur et al., 2017). Concurrently, vegetation changes influence regional land–atmosphere energy balances via altered carbon and water exchange processes within the pan-Arctic ecosystem, subsequently modulating mid-to-high latitude climate patterns (Beer et al., 2010). Consequently, a precise understanding and systematic monitoring of pan-Arctic vegetation dynamics and their driving factors (particularly those related to carbon uptake) are critical for improving projections of Arctic climate evolution under varying emission scenarios.

Previous studies have shown that long-term climate change could significantly influence terrestrial vegetation carbon assimilation through various influence pathways (Pearson, 2013). As a reactant of plant photosynthesis, CO_2 fertilization has been considered the

* Corresponding author at: College of Meteorology and Oceanography, National University of Defense Technology, Changsha 410073, China.
E-mail address: zhouhao@mail.iap.ac.cn (H. Zhou).

https://doi.org/10.1016/j.ecoinf.2025.103267
Received 15 January 2025; Received in revised form 5 June 2025; Accepted 6 June 2025
Available online 11 June 2025
1574-9541/© 2025 The Authors. Published by Elsevier B.V. This is an open access article under the CC BY-NC license (http://creativecommons.org/licenses/by-nc/4.0/).

dominant contributor to global vegetation carbon increases in recent decades. Piao et al. (2013) reported that CO_2 dominated 16 % of the increase in net primary productivity variability per 100 ppm at the global scale, especially in tropical regions. Moreover, changes in light, water and heat conditions affect vegetation growth via photosynthetic processes, such as optimal temperature ranges (Li et al., 2024), radiation balances between diffuse and direct radiation (Durand et al., 2021; Xue et al., 2024), soil moisture depletion (Liu et al., 2020) and air water loss (Green et al., 2019; Sulman et al., 2016). For example, Zhou et al. (2023) reported that diffuse radiation (with more directions) contributed up to 30 % of gross primary productivity (GPP) variability at global sites, which was significantly greater than that of direct radiation and other climatic factors. Zhong et al. (2023) reported that increasing the atmospheric vapor pressure deficit (VPD) reduced global vegetation growth through stomatal regulation, offsetting the positive CO_2 fertilization effect at the global scale. However, these studies focused primarily on the impacts of climate change on land carbon uptake, mainly at low–middle latitudes, resulting in limited exploration of the climatic drivers of greening trends across the ecologically fragile pan-Arctic region, which is constrained by high-latitude observation limitations.

With the further development of remote sensing technology, satellite-based vegetation indices (VIs) have been widely used to represent dynamic variations in terrestrial vegetation. Greener vegetation with a high chlorophyll content can absorb more visible red light and reflect more near-infrared (NIR) radiation (Hollinger, 1989). As a result, the normalized difference vegetation index (NDVI) was first calculated on the basis of the difference between the red and near-infrared bands (Tucker, 1979). However, using radiative transfer models, Sellers et al. (1992) demonstrated that vegetation-induced NIR reflectance could more reliably represent the fraction of absorbed photosynthetically active radiation than the NDVI. Therefore, Badgley et al. (2017) multiplied the NDVI by the NIR to calculate a new vegetation index, termed the near-infrared reflectance of vegetation (NIRv). Recently, Camps-Valls et al. (2021) developed a unified vegetation index called the kernel NDVI (kNDVI). By applying a particular kernel function, the kNDVI ensures that all higher-order relations between the spectral channels are accounted for, not limited to first-order interactions. Moreover, other VIs can also represent vegetation growth and greening variations, such as the enhanced vegetation index (EVI) (Huete et al., 2002) and leaf area index (LAI) (Chen and Cihlar, 1996). Like the NDVI, the EVI is derived from the red and near-infrared bands but incorporates corrections for atmospheric conditions and canopy background interference (Jiang et al., 2008), demonstrating good performance in dense vegetation canopies, particularly in tropical regions. Unlike other VIs, the LAI is always indirectly estimated using radiative transfer models and empirical relationships such as NDVI-derived algorithms; however, large uncertainties exist among various vegetation types because of limitations in parameterized processes (Lemaire et al., 2008). While these VIs have been widely used to represent terrestrial carbon dynamics at the site, regional, and global scales, it remains unclear which VI is more suitable for monitoring rapid vegetation changes (such as greening and browning) in the pan-Arctic.

This study explored the main climatic drivers of terrestrial carbon dynamics across pan-Arctic ecosystems over the past two decades via multisource measurements. Considering the unique characteristics (e.g., low-stature vegetation) of the pan-Arctic regions, three NDVI-related VIs, namely, the NDVI, NIRv and kNDVI, were selected as vegetation indicators on the basis of (1) their high sensitivity to low vegetation (such as grasslands) and (2) computational simplicity using direct satellite observations. First, the spatiotemporal variations in three satellite-based VIs (NDVI, NIRv and kNDVI) and eight climate factors were analyzed across pan-Arctic ecosystems from 2001 to 2023. Then, the correlations between the three VIs and multisource (ground- and satellite-based) estimates of pan-Arctic carbon dynamics were assessed. Finally, the individual contributions of various climate factors to terrestrial carbon dynamics in pan-Arctic ecosystems were quantified through partial correlation and ridge regression analyses.

2. Data and methods

2.1. FLUXNET observations

Ground-based observations from the global FLUXNET network were obtained via eddy covariance methods (Tramontana et al., 2016). FLUXNET is the largest worldwide network providing half-hourly ecosystem flux measurements, integrating regional networks such as ICOS, AmeriFlux, AsiaFlux, ChinaFLUX, and TERN-OzFlux (Jung et al., 2019). This network provides nearly 200 in situ stations from more than 30 countries with more than 1 year of continuous observations, including ecosystem-scale data on biosphere–atmosphere exchanges of carbon dioxide, water and energy between the biosphere and atmosphere, as well as other meteorological and biological measurements (Pastorello et al., 2020). Eighty-three sites with more than one year of carbon fluxes observations were selected from the FLUXNET2015 databases in pan-Arctic regions ($>$ 45°N latitude) among seven plant functional types (PFTs), including cropland (CRO), deciduous broadleaf forest (DBF), evergreen needleleaf forest (ENF), grassland (GRA), mixed forest (MF), open shrubland (OSH), and permanent wetland (WET) (Table S1). Moreover, to reduce uncertainties in net ecosystem exchange-derived methods, ensemble GPP values (unit: g C m^{-2} day^{-1}) were calculated as the average of the daytime (GPP_DT_VUT_MEAN) and nighttime (GPP_NT_VUT_MEAN) methods. The gridded VI data were interpolated to site-level spatiotemporal resolutions for comparison.

2.2. Gridded meteorology data

Meteorological data were obtained from the Modern-Era Retrospective Analysis for Research and Applications Version 2 (MERRA-2) reanalysis, including total precipitation, air temperature (AT), land surface temperature (LST), solar radiation and vapor pressure deficit (VPD). Furthermore, diffuse and direct radiation were reconstructed by combining the satellite-based diffuse radiative fraction (DF) from Ryu et al. (2018) with the MERRA-2 shortwave radiation data:

$$Direct = SW_{MERRA-2} \cdot (1 - DF) \quad (1)$$

$$Diff = SW_{MERRA-2} \cdot DF \quad (2)$$

Moreover, soil moisture data were obtained from the GLDAS_NOAH025_M product, and spatial atmospheric CO_2 concentration data were obtained from the Global Atmospheric CO_2 Concentration Raster Simulation Dataset (GACRS) (Hou et al., 2021). Global annual land cover data were sourced from the MCD12Ql product of MODIS retrievals (Fig. S1). All the gridded meteorological data were downscaled to a spatial resolution of 0.5° and an 8-day temporal resolution for the 2001–2023 period across the pan-Arctic region. In this study, pan-Arctic regions were defined as 180°W–180°E and 45°N–90°N following the methods of Zhang et al. (2024a), as 45°N has been widely recognized as the biogeographic boundary for Arctic vegetation changes (Park et al., 2016).

2.3. Satellite-based vegetation index

Three vegetation indices (NDVI, NIRv, and kNDVI) were derived from MODIS MOD09A1 surface reflectance data for pan-Arctic analysis (2001−2023). The reflectance data underwent mosaicking, cloud masking, and region-of-interest extraction prior to VI calculation. VI processing was implemented in the Google Earth Engine (GEE) (Gorelick et al., 2017), a cloud-based platform that provides access to satellite archives and high-performance geospatial computations.

The formulas for the three VIs are as follows:

$$NDVI = \frac{NIR - Red}{NIR + Red} \tag{3}$$

$$NIRv = NDVI^{*}NIR \tag{4}$$

$$kNDVI = \tanh\left(\left(\frac{NIR - Red}{2\sigma}\right)^{2}\right) \tag{5}$$

where σ is a length-scale parameter determined empirically. To quantify the sensitivity of the index to sparsely/densely vegetated regions, we took $\sigma = 0.5(NIR + Red)$ following Camps-Valls et al. (2021). Solar-induced chlorophyll fluorescence (SIF) is the escape of light released by plants during photosynthesis and can be used for regional validation. The Global Orbiting Solar-Induced Fluorescence (GOSIF) dataset developed by Li and Xiao (2019) was utilized through the fusion of satellite observations and machine learning. For annual trends, the Sen + Mann–Kendall method was used to calculate the significance levels of the trends (see Supplementary Information 1). Trends were classified into 9 categories, which are represented by the numbers −4 to 4 in Fig. S4, and the specific division criteria are shown in Table S2.

2.4. Partial correlation and ridge regression analysis

This study used partial correlation and ridge regression analysis (which works best in the pan-Arctic region) to detect the effects of climate factors on NIRv changes in pan-Arctic ecosystems. The partial correlation approach can be used to accurately assess the degree and direction of correlation between two variables by removing the collinearity between other input variables (Zhong et al., 2021). To address multicollinearity in regression modeling (Chen et al., 2017), ridge regression with a penalty parameter λ (Hoerl and Kennard, 1970) was adopted. All variables were normalized prior to constructing the ridge model. The ridge regression models were constructed as follows:

$$Y = \sum_{i=1}^{n} a_i x_i + b \tag{6}$$

$$a_i = \left(x_i^T x + \lambda I\right)^{-1} x_i^T Y \tag{7}$$

The optimal λ (ranging from 10^{-5} to 10^{3}) was selected by minimizing the mean absolute percentage error. The relative and absolute contributions of the climatic factors to the NIRv could be determined using the regression coefficients of the ridge regression and the trend of the variables following the method suggested by Zhao et al. (2023).

$$\gamma_{ci} = a_i \bullet X_{i_{trend}} \tag{8}$$

$$\gamma_{aci} = \frac{\gamma_{ci}}{Y_{n_{trend}}} \cdot Y_{trend} \tag{9}$$

$$\gamma_{rci} = \frac{|\gamma_{ci}|}{\sum_{i=1}^{8} |\gamma_{ci}|} \tag{10}$$

The influence of the actual trends of various climatic factors on NIRv variations was considered by calculating absolute and relative contributions. Specifically, absolute contributions could indicate positive or negative climatic impacts, whereas the relative contributions indicate only the relative magnitudes of various climatic factors on the pan-Arctic NIRv (Xie et al., 2020).

Model performance was validated via variance inflation factor (VIF) reduction (Fig. S5) and high prediction–observation correlation (R = 0.95; Fig. S6).

3. Results

3.1. Spatiotemporal variations in three VIs

The spatiotemporal variations in three VIs across the pan-Arctic were explored (Fig. 1). During 2001–2023, all VIs presented similar spatial patterns, with higher values over boreal Asia and Europe (55°N–60°N), corresponding to forest-dominated regions (Fig. S1), and lower values at higher latitudes (Fig. 1a–c). Moreover, the NDVI, NIRv and kNDVI showed positive trends of 0.0005 ± 0.0008 yr^{-1}, 0.0017 ± 0.0014 yr^{-1} and 0.0009 ± 0.0013 yr^{-1}, respectively (Fig. 1d-f), covering 68.22 %, 74.49 % and 69.71 % of the total pan-Arctic grid cells, respectively (Fig. 1g-i). This trend of rapid vegetation growth is significantly greater than that at mid-latitudes (where only 51.80 % of Eurasia is significantly greener) (Wang et al., 2024) and on the Tibetan Plateau (greening was found in 55 % of the landmass) (Wu et al., 2024). Owing to the wide variation in climatic conditions in the pan-Arctic region, the uncertainty of this vegetation index change is influenced mainly by its spatial distribution. For spatial patterns, visible greening (referred to as increases in VIs) was detected in northeast Asia and Europe over time, whereas localized browning occurred in the low pan-Arctic regions (Fig. 1g-i). Within the Arctic (>66.5°N), all vegetation types showed an increasing trend, with significant growth in approximately 40 % of the area and no significant browning areas, which corroborates previous findings (Heijmans et al., 2022). The NIRv presented stronger greening signals than did the NDVI and kNDVI from 2001 to 2023. Overall, all VIs revealed heterogeneous spatial patterns and robust greening trends across most pan-Arctic regions. Climatic factors displayed distinct spatiotemporal variations (Figs. S2–S3; Supplementary Information Section 2).

3.2. Validation of the applicability of satellite-based VIs

The applicability of three satellite-based VIs for characterizing GPP variations was validated at FLUXENT sites (Figs. 2 and 3). Among the 83 flux sites, three VIs presented positive correlation coefficients (R values, $p < 0.05$) ranging from 0.59 to 0.63, with the highest R value of 0.63 for the NIRv and the lowest R value of 0.59 for the NDVI. These moderate correlations may arise from (1) spatial scale mismatches between coarse-resolution (500-m) VI data and ground-based flux footprints and (2) incomplete representation of subpixel vegetation heterogeneity. For all plant functional types, the NIRv demonstrated stronger correlations (R = 0.63 ± 0.32) than did the NDVI (R = 0.59 ± 0.36) and kNDVI (R = 0.60 ± 0.38), peaking in deciduous broadleaf forests (R = 0.81–0.94) and showing the weakest performance in croplands (R = 0.47–0.62). Canopy structural differences further amplified the correlations, with forests exhibiting a greater R (0.74 ± 0.14) than nonforest ecosystems did (0.68 ± 0.12) for the three VIs. For long-term vegetation dynamics (> 10 years), the observed GPP displayed increasing trends at most sites, with all VIs showing strong agreement (R = 0.683–0.689; peaking at 0.689 for the NIRv; Fig. 3a-c). Moreover, the NIRv exhibited stronger greening trends (0.53 ± 0.87 % yr^{-1}) than did the NDVI (0.27 ± 0.49 % yr^{-1}) and kNDVI (0.40 ± 0.75 % yr^{-1}), which aligns with ground-based GPP trends (0.57–0.73 % yr^{-1}; Fig. 3d).

The capacity of three VIs to represent the pan-Arctic SIF product was further investigated at regional scales (Figs. 4 and 5). The NDVI (R = 0.53 ± 0.13), NIRv (R = 0.56 ± 0.12) and kNDVI (R = 0.51 ± 0.11) demonstrated moderate correlations with SIF at low–mid-pan-Arctic latitudes but exhibited weak relationships ($R < 0.1$) at high latitudes (Fig. 4a-c), likely attributable to subtle pigment variations undetectable by VI sensors. The three VIs also showed comparable performance in capturing SIF patterns (Fig. 4d-f). For temporal trends, the NIRv aligned with the SIF trends across 72.87 % of the pan-Arctic grids (59.41 % positive, 13.46 % negative), surpassing the NDVI (67.09 %) and kNDVI (68.14 %) (Fig. 5a-c). Moreover, compared with the NDVI and kNDVI, the NIRv also significantly improved the representation of the SIF trends

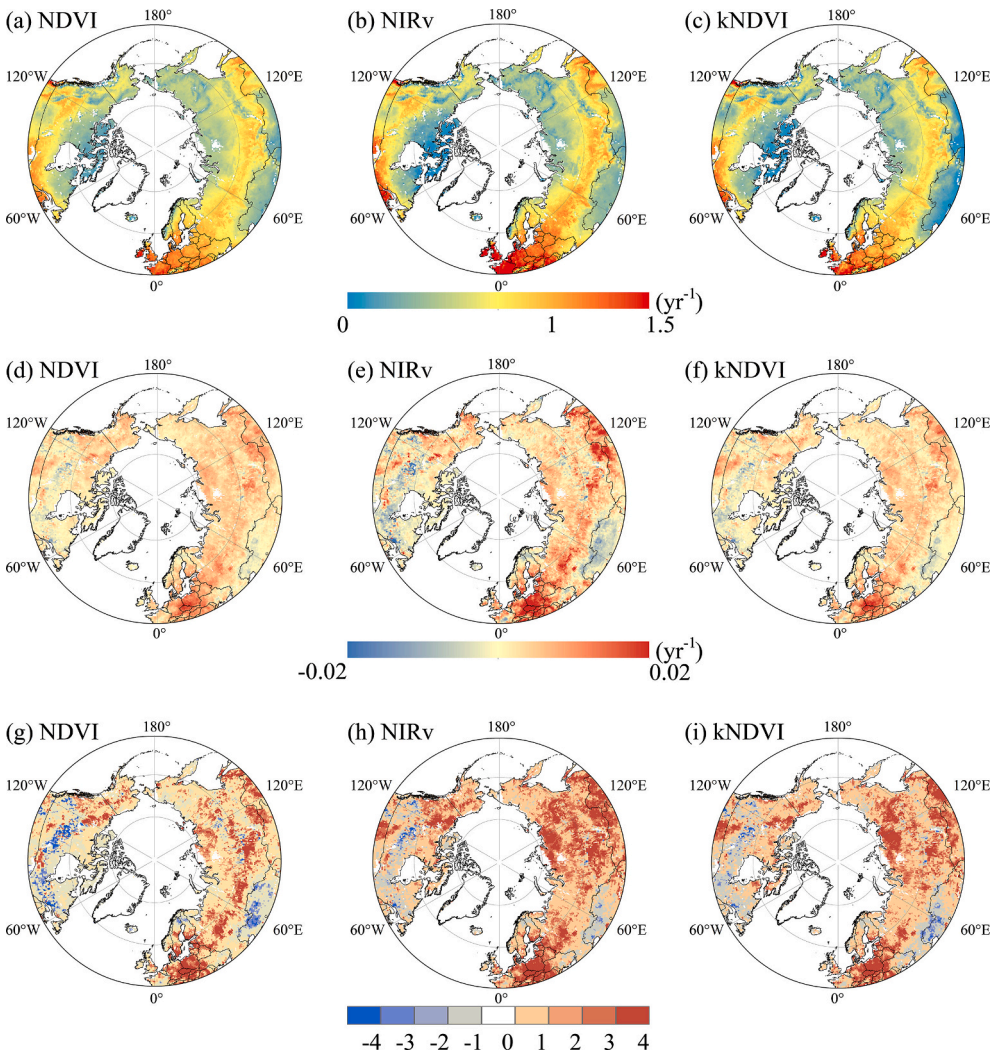

Fig. 1. (a-c) Spatial patterns, (d-f) temporal trends and (g-i) significant levels of vegetation indices (VIs) in the pan-Arctic region from 2001 to 2023. The numbers in g-i from −4 to 4 represent various trend levels, following that order: extremely significant decrease, significant decrease, slightly significant decrease, no significant decrease, no change, no significant increase, slightly significant increase, significant increase and extremely significant increase.

among the ten vegetation types (Fig. 5d). For example, the SIF showed the highest positive trends, up to 0.48 ± 1.29 % yr^{-1}, which was consistent with 0.39 ± 0.97 % yr^{-1} for the NIRv and higher than 0.17 ± 0.56 % yr^{-1} and 0.28 ± 0.79 % yr^{-1} for the NDVI and kNDVI, respectively. Both site-level and gridded validations identified the NIRv as the optimal proxy for pan-Arctic carbon dynamics, leading us to select the NIRv for subsequent analysis of climatic drivers.

3.3. Partial correlation analysis between the NIRv and climatic factors

Individual impacts of climatic factors on terrestrial carbon uptake were isolated through partial correlation analysis (Fig. 6 and Table 1). From 2001 to 2023, there was a positive correlation between CO_2 and the NIRv (0.13 ± 0.34) across all grids, accounting for 64.18 % of the total grids (Fig. 6a), indicating strong fertilization effects on terrestrial carbon uptake due to increasing CO_2 concentrations. Diffuse and direct radiation showed weaker partial correlations (−0.11 ± 0.27 and 0.10 ± 0.28, respectively) with the pan-Arctic NIRv. Precipitation had weaker responses to the NIRv than did soil moisture (Fig. 6d), and positive partial correlation coefficients (0.07 ± 0.29) between soil moisture and the NIRv were found, especially in boreal Asia (Fig. 6e). Moreover, increases in the AT contributed stronger positive NIRv responses than other meteorological factors did over 87.3 % of the pan-Arctic grids (Fig. 6f), which suggests that photosynthesis is more sensitive to temperature in the cold-limited pan-Arctic region. Similar to the AT, the LST showed positive partial correlations (0.23 ± 0.22) with the NIRv across most pan-Arctic areas, reflecting the significant effects of warming on both the extension of the vegetation growing season and summer photosynthesis. For VPD, the NIRv presented positive responses to increases in VPD at high latitudes but negative responses in low pan-Arctic regions (Fig. 6g). Compared with those in the low pan-Arctic region (Fig. 6h, 45°N–60°N), most climatic factors, such as CO_2 and AT, presented stronger correlations than did those in the high pan-Arctic region (Fig. 6h, 60°N–90°N), which is related to differences in plant functional type (Fig. S1 and Fig. S7).

3.4. Ridge regression analysis between the NIRv and climatic factors

The absolute contributions of climatic factors to terrestrial NIRv variability (2001–2023) were quantified using ridge regression analysis (Fig. 7 and Table 1). Increasing CO_2 contributed the strongest increase in the NIRv (0.002 ± 0.005) in the pan-Arctic regions (Fig. 7a), whereas negative effects were detected in the low-pan-Arctic regions. Solar radiation (including diffuse and direct radiation) had no significant effects on the changes in the NIRv due to minimal surface radiation variations (Fig. 7b and c). Precipitation and soil moisture contributions presented

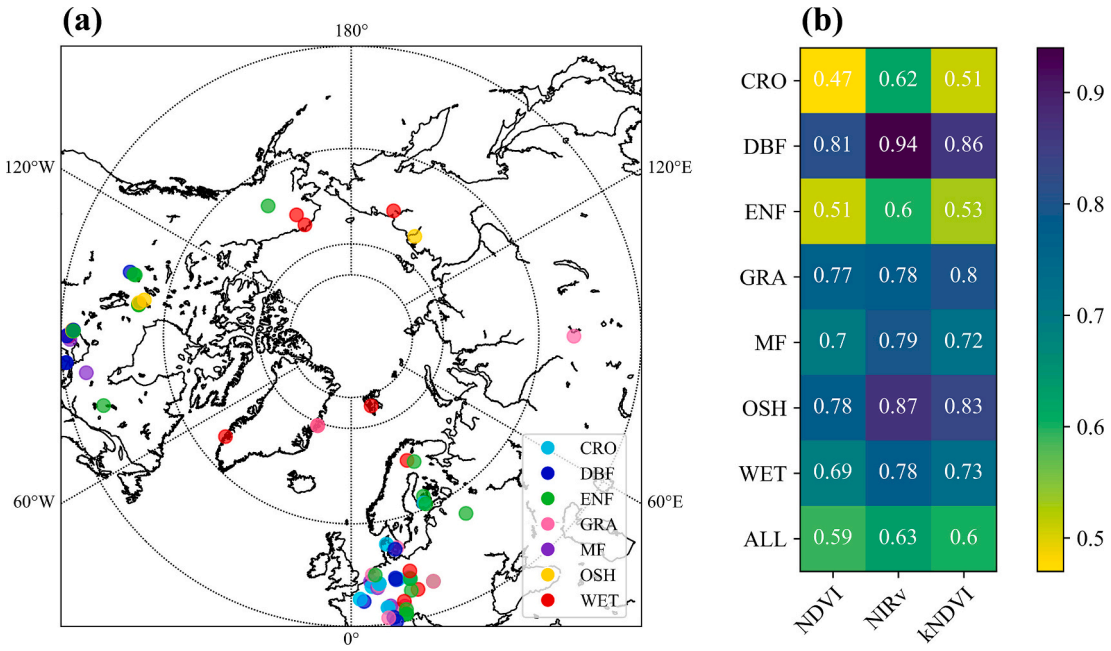

Fig. 2. (a) Distribution of FLUXNET sites in the pan-Arctic region and correlation coefficients between three VIs and site-level gross primary productivity (GPP) among various plant functional types (PFTs). The PFTs included cropland (CRO), deciduous broadleaf forest (DBF), evergreen needleleaf forest (ENF), grassland (GRA), mixed forest (MF), open shrubland (OSH), and permanent wetland (WET).

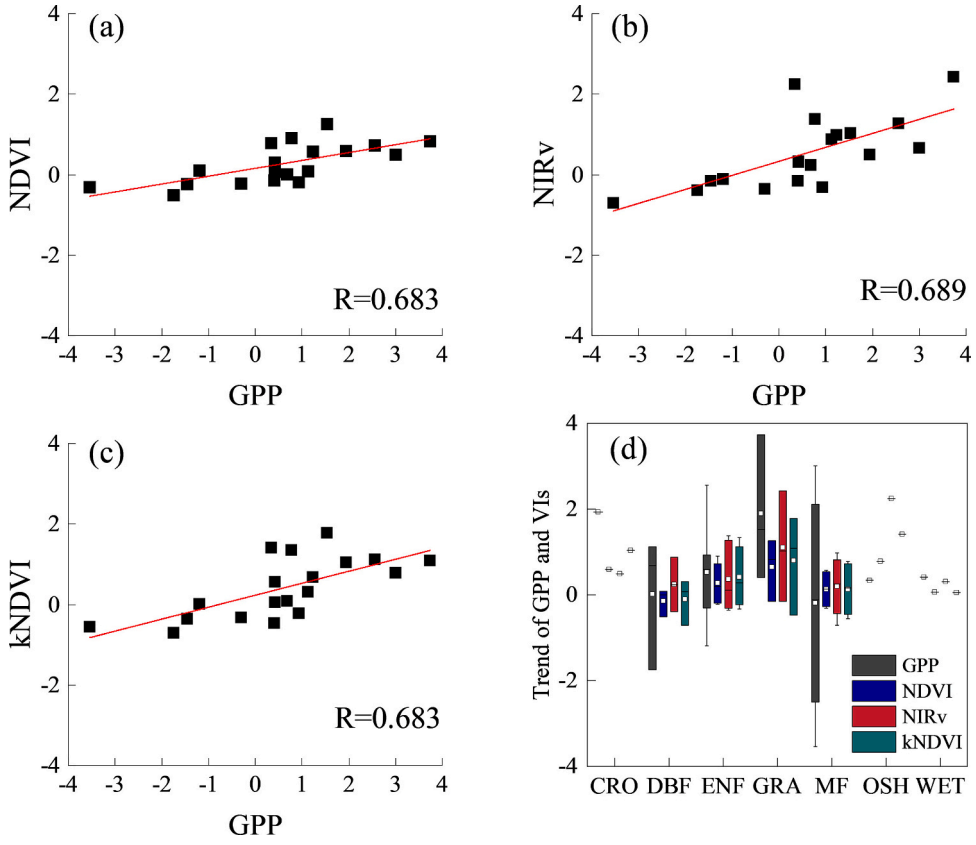

Fig. 3. Comparison of (a-c) temporal trends between three VIs and site-level GPP and (d) their performance among various PFTs. All trends were calculated by the normalized values of VIs and GPP, and their units are % yr^{-1}. These ground-based sites included more than 10 years of observations of carbon fluxes (e.g., GPP). The boxplots are shown to indicate differences in all VIs among various PFTs.

similar spatial patterns with negative effects on the NIRv due to soil water saturation in high-pan-Arctic regions (Fig. 7d and e). AT increases caused positive NIRv values (0.0005 ± 0.003) primarily in Europe and boreal Asia (Fig. 7f and Fig. S3f). LST enhancements drove minor increases in the NIRv (0.00008 ± 0.001) (Fig. 7h). Increasing VPD promoted NIRv changes (0.002 ± 0.01) in high pan-Arctic regions (Fig. 7i)

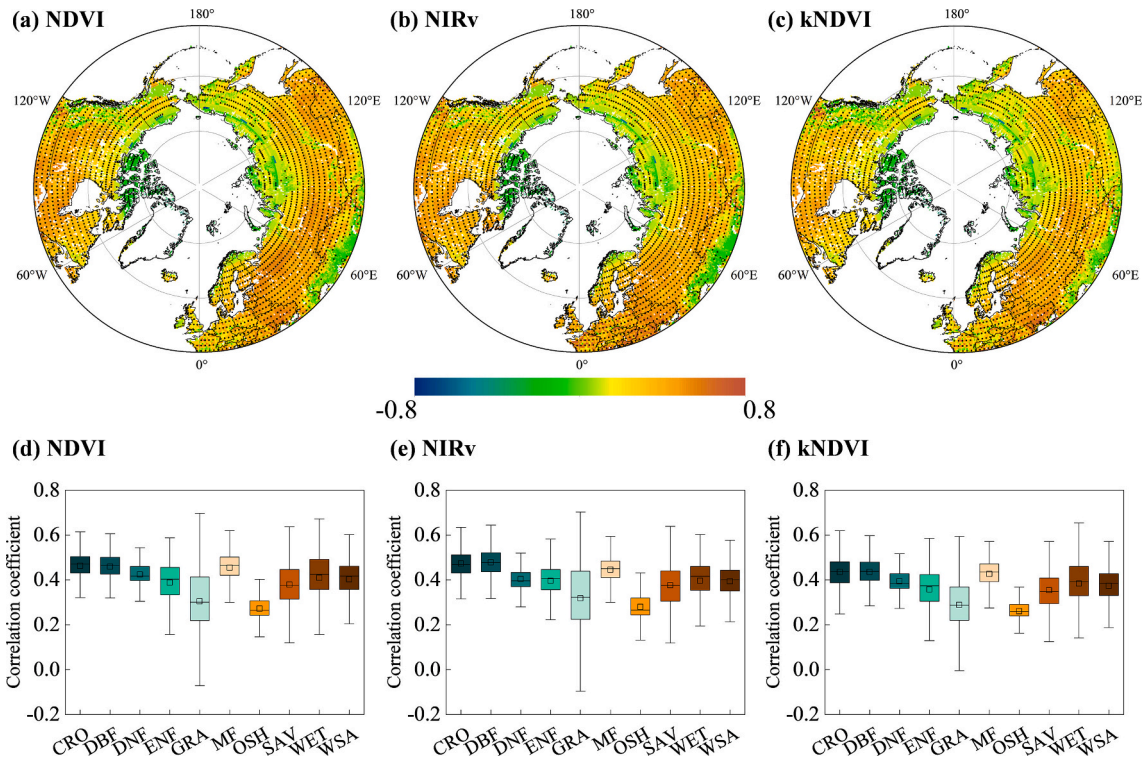

Fig. 4. (a-c) Correlation coefficient between three VIs and the GOSIF product and (d-f) comparison among various PFTs in the pan-Arctic region from 2001 to 2023. The black dots indicate significant correlations ($p < 0.05$).

but weakened the NIRv (−0.0002 ± 0.003) in Europe (Fig. 7g). Moreover, decreased VPD enhanced the NIRv in Mongolia (Fig. S3g and Fig. 7g). From low to high pan-Arctic ecosystems, vegetation greening trends (NIRv increases) were more sensitive to increasing CO_2, AT and VPD under global warming, despite reduced CO_2 fertilization (Fig. 7h and i). Among the vegetation types, CO_2 presented the highest NIRv variability (0.0036 ± 0.0048) in mixed forest and the lowest (0.001 ± 0.005) in grasslands (Fig. S6a). Solar radiation, precipitation and LST had negligible effects across plant functional types (Fig. S8b-S8d and S8g). Soil moisture and VPD had significant negative effects on croplands but had no significant effects on other plant functional types. AT contributed substantially to cropland (0.0026 ± 0.0046), particularly in Europe and boreal Asia (Fig. S1).

In addition to absolute contributions, this study also quantified the relative contributions of climatic factors to terrestrial NIRv variability in the pan-Arctic regions (Fig. 8). Among the climatic factors, CO_2 dominated the NIRv variability (34.5 ± 18.6 %) over most areas, especially in boreal Asia (Fig. 8a), substantially exceeding the radiation effects (Fig. 8b and c). Precipitation controlled the NIRv variability by 8.6 ± 9.1 % (Fig. 8d), especially in the low-latitude pan-Arctic with positive precipitation trends (Fig. S4). Soil moisture and VPD contributed 10.9 ± 11.1 % and 11.2 ± 12.1 %, respectively, to plant growth, indicating the importance of water availability to plant growth (Fig. 8e and g). The AT caused NIRv variability of up to 15.1 ± 14.4 %, peaking at 27.6 ± 13.5 % in Europe (Fig. 8f). Moreover, the LST contributed 6.7 ± 7.2 % to the pan-Arctic NIRv variability, with the highest values (>20 %) occurring in Canada (Fig. 8h). Compared with other climatic factors, CO_2 had the greatest relative contribution across various plant functional types, peaking at 34.4 ± 19.4 % for deciduous needleleaf forest and showing the lowest value (27.7 ± 17.7 %) for cropland (Fig. S9a). Diffuse radiation, direct radiation and precipitation did not significantly differ among the various plant functional types (Fig. S9b-S9d). Soil moisture exhibited relatively high contributions (14.2 ± 13.4 % and 14.7 ± 13.2 %, respectively) for grassland and open shrubland (Fig. S9e), despite negative absolute effects (Fig. 7). AT had the greatest contribution (19.6 ± 16.4 %) for cropland but only 9.5 ± 8.9 % for deciduous broadleaf forest (Fig. S9f). LST contributed the most to wetland (8.8 ± 7.1 %) and the least to cropland (4.5 ± 5.4 %). However, VPD had the strongest effect (9.8 ± 9.1 %) on deciduous needleleaf forest (Fig. S9g).

4. Discussion

4.1. Advantages of the NIRv for representing pan-Arctic carbon dynamics

This study explored the correlations between three VIs and ground/satellite-based carbon dynamics across pan-Arctic ecosystems, revealing the superior performance of the NIRv in capturing vegetation carbon dynamics, particularly greening trends, compared with the NDVI and kNDVI (Figs. 1–5). Under low light availability at high latitudes, pan-Arctic vegetation dynamics are more sensitive to temperature and water conditions than are tropical ecosystems (Pearson, 2013; Zhang et al., 2022), leading to more vegetation types with simple canopy structures (e.g., grassland and shrubland) (Heijmans et al., 2022; Oehri et al., 2022). Therefore, pan-Arctic vegetation with simple canopy structures exhibits faster photosynthetic responses to environmental changes at the leaf scale, resulting in higher NIR reflectance (Badgley et al., 2017). Previous studies have shown that NIR reflectance can better indicate the fraction of photosynthetically active radiation than NDVI (Sellers, 1987), particularly when separating vegetation signals from non-vegetated background reflectance. The NIRv is more sensitive to plant growth in areas with sparse leaf cover than are the NDVI and kNDVI because of its stronger response to vegetation-specific reflectance (Zheng et al., 2024). In pan-Arctic terrestrial ecosystems, grasses, shrubs and tundras (with low heights and simple structures) dominate due to harsh climatic conditions (Fig. S1). These vegetation types have high photochemical capacity and absorb more direct than diffuse radiation to avoid light saturation (Maes et al., 2024; Zhao et al., 2022), enhancing NIRv sensitivity through direct light reflectance (Badgley et al., 2019). Similarly, this study revealed that the NIRv captures greening trends

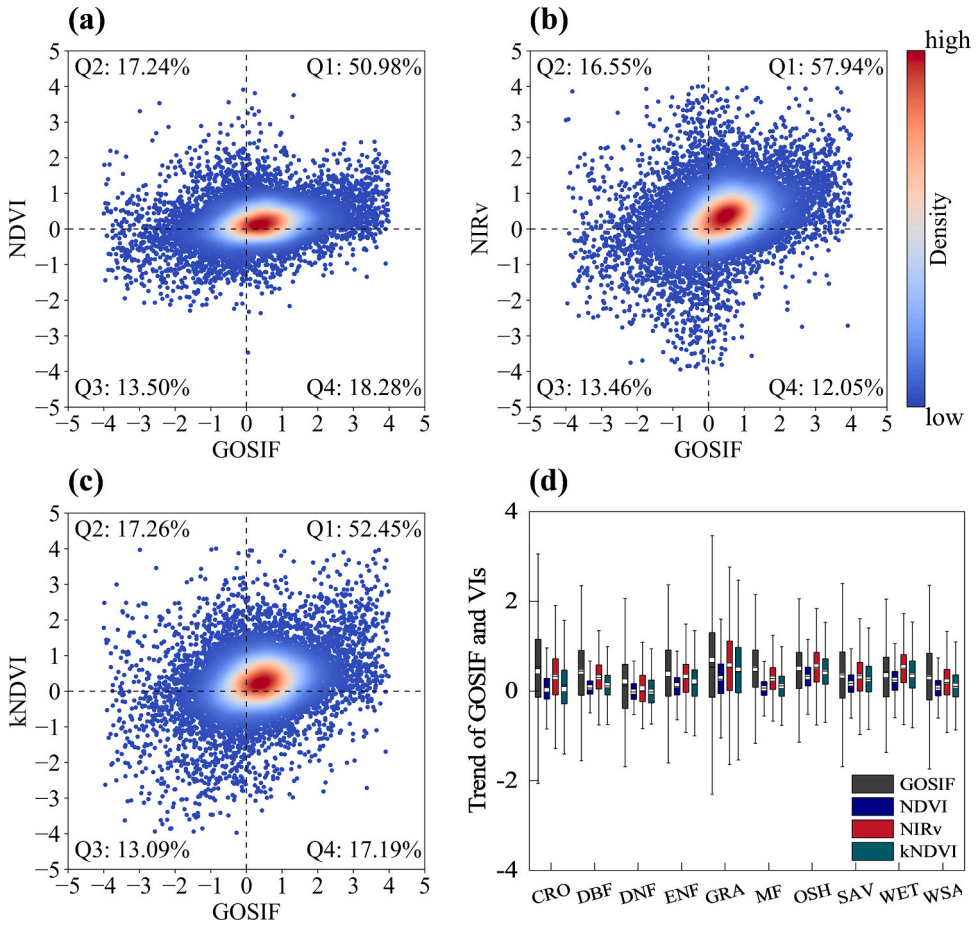

Fig. 5. (a-c) Comparison of the temporal trends between three VIs and GOSIF products and (d) performance among various PFTs. All trends were normalized for comparison, and the units are % yr^{-1}. For a-c, the color gradients represent low (blue) to high (red) density points. (For interpretation of the references to color in this figure legend, the reader is referred to the web version of this article.)

better than the NDVI and kNDVI do in nontree species with simple canopy structures (Figs. 3 and 5). For example, the NIRv presented positive trends up to 1.17 ± 1.14 % yr^{-1}, much higher than the 0.56 ± 0.59 % yr^{-1} and 0.77 ± 0.95 % yr^{-1} for the NDVI and kNDVI, respectively, for grasslands, open shrublands and permanent wetlands, which was closer to the 1.29 ± 1.46 % yr^{-1} of the site-level GPP trends at the FLUXNET sites (Fig. 3d). However, the NIRv showed similar annual trends to those of the other VIs in forests (deciduous broadleaf forest, evergreen needleleaf forest and mixed forest; Fig. 3d).

4.2. Importance of climatic factors to pan-Arctic NIRv variations

This study explored climatic effects on terrestrial NIRv variations across pan-Arctic ecosystems using partial correlation and ridge regression analyses from 2001 to 2023 (Figs. 6–8). The results revealed that CO_2 fertilization effects dominated the pan-Arctic greening trends, whereas heat and water conditions also significantly influenced terrestrial carbon dynamics (Figs. 6–8). Previous studies have shown that CO_2 fertilization effects have controlled global land carbon uptake increases over recent decades (Schimel et al., 2015), although the CO_2 fertilization efficiency has decreased (Wang et al., 2020). The analysis revealed positive partial correlations between CO_2 and NIRv across most pan-Arctic regions (Fig. 6a), with the ridge regression showing dominant CO_2 contributions (34.5 %) exceeding those of other climatic factors (Fig. 8). However, such CO_2 fertilization rates have decreased to 24.2 % in Europe despite high anthropogenic emissions, potentially linked to photosynthetic saturation at elevated CO_2 levels (Tomimatsu and Tang, 2016). Thus, heat and water conditions such as increasing AT and VPD dominated the NIRv variability in the same low-latitude regions (Fig. 8h), despite counteracting effects from AT (Fig. 7f) and VPD (Fig. 7g). Owing to limited solar radiation, the AT is always lower than the optimal temperature for plant photosynthesis (the temperature threshold for maximum photosynthesis), resulting in enhanced vegetation carbon assimilation, with the AT and LST increasing in pan-Arctic ecosystems (Yuxi et al., 2024). Similarly, results demonstrated significant positive correlations between pan-Arctic warming and NIRv across most regions (Fig. 6f and 7f). Rising temperatures accelerate enzymatic processes in photosynthesis, improving the vegetation growth efficiency through earlier growing season onset and extended season length. In addition, while warming accelerates soil organic matter decomposition and permafrost thaw (releasing CO_2 and CH_4), it simultaneously enhances vegetation carbon sequestration. Seasonal freeze–thaw cycles alter soil hydrothermal conditions, with LST fluctuations significantly affecting vegetation dynamics (Li et al., 2025; Zhang et al., 2024b). Although the LST was positively correlated with vegetation growth, this relationship was constrained by limited interannual AT variability. Diffuse radiation contributed more strongly (7.1 %) than direct radiation did (5.9 %) because of higher light use efficiency (Siriwardana and Kume, 2025), a phenomenon modulated by aerosol- and cloud-driven shifts in radiation partitioning.

In addition to CO_2 and temperature effects, the results also revealed that soil moisture and VPD presented diverse NIRv responses through water regulation under climate change over the past 23 years. Water availability directly affects plant growth and photosynthesis via atmospheric aridity and soil moisture through leaf and root processes (Novick et al., 2016a; Sulman et al., 2016). Increased soil moisture enhances root

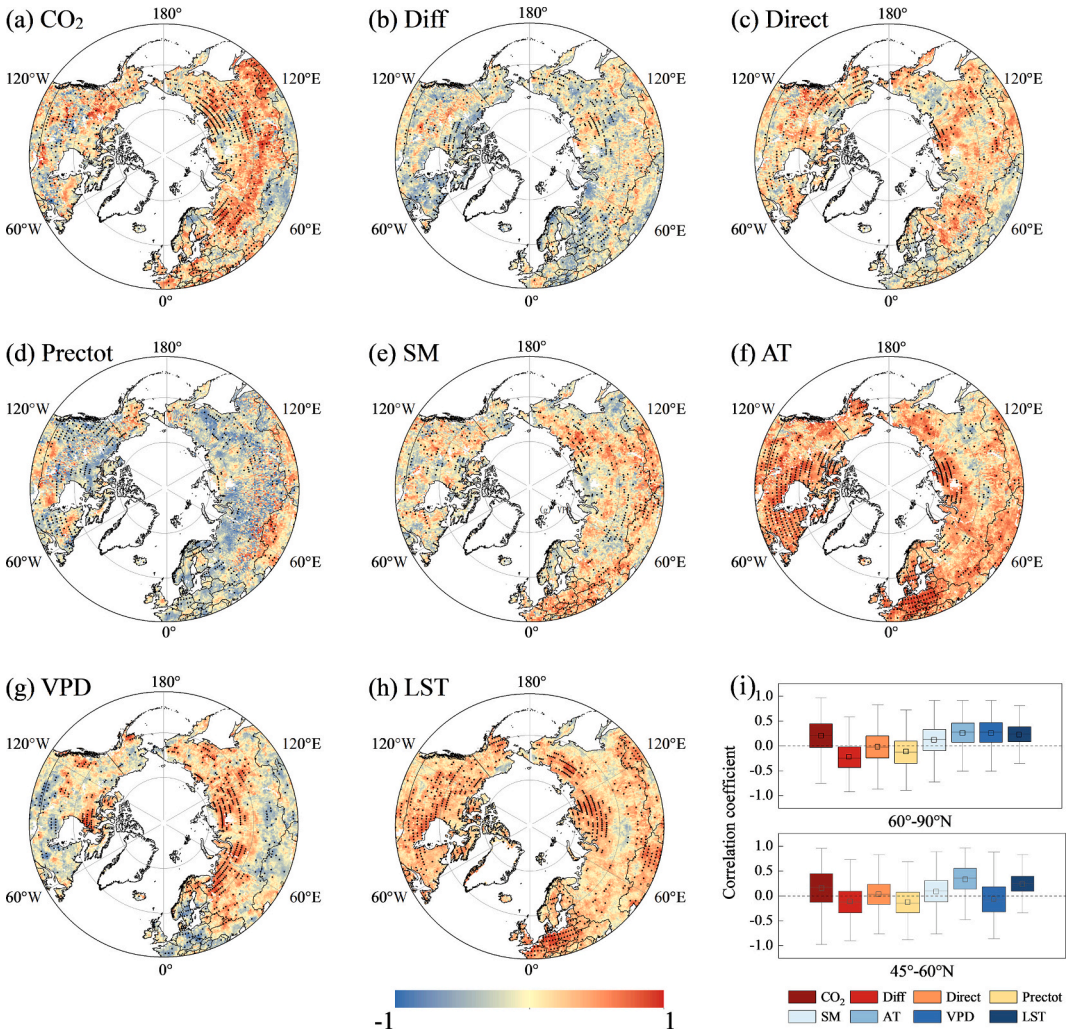

Fig. 6. (a-g) Spatial patterns of partial correlation coefficients between the NIRv and climatic factors and (h-i) their differences among various latitudes in the pan-Arctic region from 2001 to 2023. The climatic factors included carbon dioxide (CO_2), diffuse radiation (Diff), direct radiation (Direct), total precipitation (prectot), soil moisture (SM), air temperature (AT), vapor pressure deficit (VPD) and land surface temperature (LST). The dots indicate the pixels with regression results that passed the test of significance ($P < 0.05$). The latitudes are divided into 45°-60°N (h, low pan-Arctic) and 60°-90°N (I, high pan-Arctic).

Table 1
Summary of the relationships between climatic factors and the NIRv.

Climatic factors	Partial correlation coefficient	Absolute contribution	Relative contribution
CO_2	0.13 ± 0.34	0.002 ± 0.005	34.5 ± 18.6 %
Diffuse radiation	−0.11 ± 0.27	−0.0002 ± 0.001	7.1 ± 7.9 %
Direct radiation	0.10 ± 0.28	−0.0002 ± 0.001	5.9 ± 6.8 %
Precipitation	−0.15 ± 0.34	−0.0003 ± 0.002	8.6 ± 9.1 %
Soil moisture	0.07 ± 0.29	−0.0003 ± 0.002	10.9 ± 11.1 %
AT	0.32 ± 0.27	0.0005 ± 0.003	15.1 ± 14.4 %
VPD	0.06 ± 0.31	0.0003 ± 0.002	11.2 ± 12.1 %
LST	0.23 ± 0.22	0.00008 ± 0.001	6.7 ± 7.2 %

water uptake, promoting plant growth and leaf photosynthesis (Konings et al., 2017). The analysis revealed positive soil moisture–NIRv correlations in most pan-Arctic regions (Fig. 6e), indicating that the regional NIRv increases with soil moisture (Figs. 7e and S3e). However, these effects may be limited under high soil water contents (Zhang et al., 2023). Compared with soil moisture, VPD as a result of air water loss showed opposing NIRv responses between low and high pan-Arctic regions (Fig. 6g), with negative (positive) correlations with NIRv in low (high) pan-Arctic regions. As the temperature increases, the saturated water vapor pressure increases exponentially, increasing VPD more rapidly than the temperature itself. This nonlinearity implies that warmer ecosystems may experience disproportionately higher VPD under future warming, potentially intensifying water stress despite uniform temperature changes (Adams et al., 2009). Previous studies have shown that increased VPD can reduce plant photosynthesis and carbon assimilation through stomatal closure under dry conditions (Novick et al., 2016a, 2016b). However, this inhibition may reverse under low background VPD (Woodruff et al., 2010), as stomatal opening is stimulated by moderate aridity (Sellin et al., 2017). Zhong et al. (2023) identified an optimal VPD range (0.35–0.40 kPa) for leaf photosynthesis using satellite data. Zhou et al. (2023) similarly reported that site-level GPP showed nonlinear responses to VPD changes, with an optimal VPD ranging from 0.2 to 0.3 kPa, with machine learning models at global FLUXNET sites. As a result, VPD increases the NIRv in high pan-Arctic regions (background VPD < threshold; Fig. S2) but suppresses the NIRv in low pan-Arctic ecosystems (Fig. 7h and i). Similarly, Yuan et al. (2019) reported that VPD was positively correlated with the satellite-based leaf area index over high latitudes from 1982 to 2015, indicating positive contributions of increased VPD to high-latitude vegetation productivity.

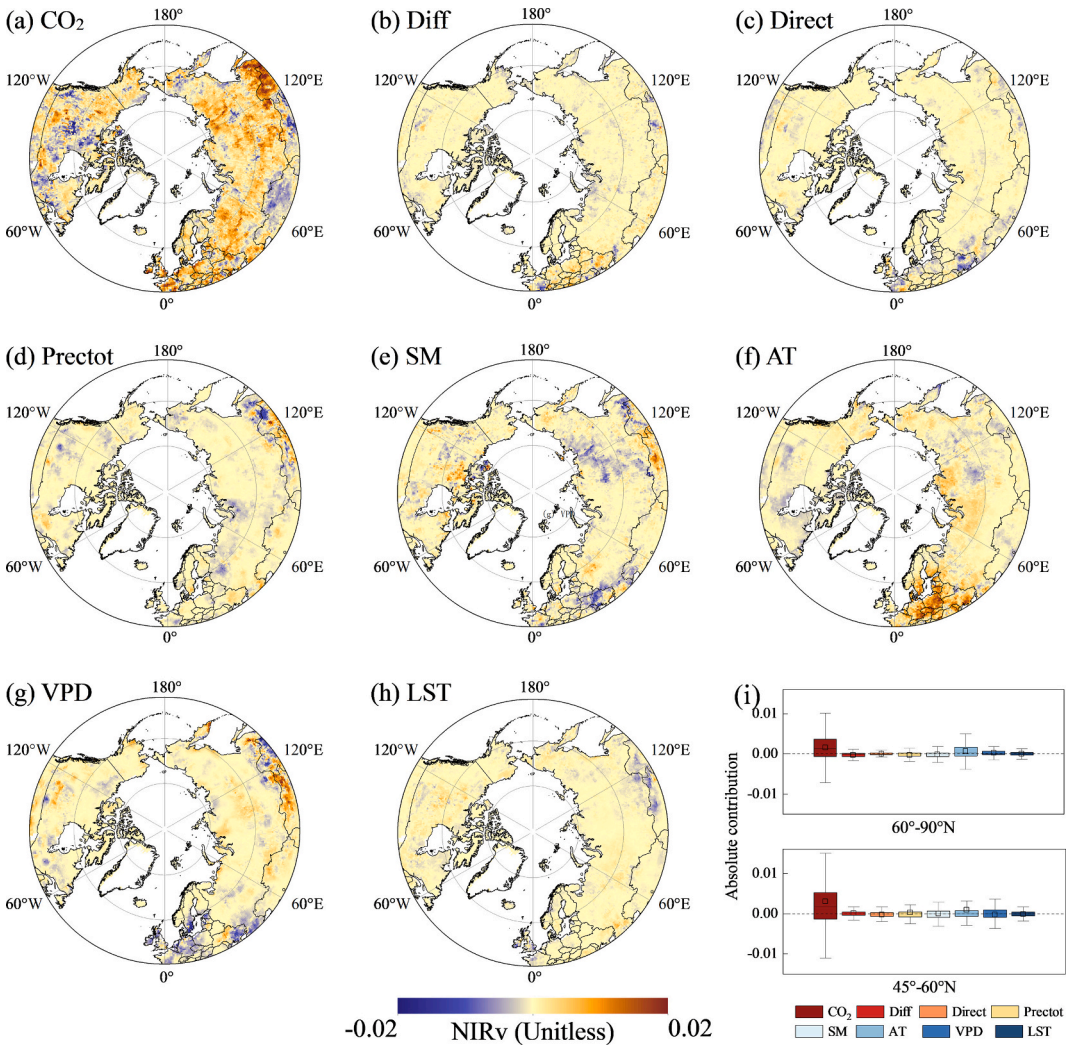

Fig. 7. Absolute contributions of seven climatic factors to the NIRv in the pan-Arctic region from 2001 to 2023. The latitudes are divided into 45°-60°N (h, low pan-Arctic) and 60°-90°N (i, high pan-Arctic).

4.3. Uncertainties and limitations

There are several uncertainties and limitations in this study, as follows: (1) The spatial heterogeneity of flux sites may influence the effectiveness of three VIs on pan-Arctic terrestrial carbon uptake. For example, most sites (> 95 %) are located in Europe and America, and very few sites are located in boreal Asia with high tree cover (Fig. 2a). As an alternative, gridded SIF products were used to represent regional carbon assimilations, with results confirming the robustness of NIRv for representing pan-Arctic vegetation carbon dynamics at regional scales (Figs. 3 and 4). (2) The neglect of human activities such as irrigation and management may have influenced our results for croplands in low Pan-Arctic areas (Fig. S1). However, the area of croplands is smaller than those of grasslands and shrublands, so this neglect has a minimal effect on the main climatic drivers. (3) Partial correlation and ridge regression address climatic factor collinearity (e.g., radiation–temperature; Li et al., 2023) but ignore interactions. Our recent study discussed the main and interactive effects of climatic factors on site-level GPP at the global FLUXNET and reported that the main effects of climatic factors were much stronger than their interactions (Zhou et al., 2023). Therefore, neglecting interactions with climatic factors may have only limited effects on our results. (4) Using only the NDVI/NIRv/kNDVI excluded other indices (e.g., MSAVI/SAVI). Future work will explore other VIs for pan-Arctic carbon dynamics. (5) Site-level studies have shown that the biodiversity of Arctic tundra, such as lichens (Erlandsson et al., 2023), can influence terrestrial vegetation variations (Crichton et al., 2022; Nakatsubo et al., 2023; Zeng et al., 2021), but neglecting some vegetation types had a limited impact on the results. This study examined ten vegetation types (Fig. S1) to distinguish differences in climatic drivers across various vegetation cover types.

5. Conclusions

This study first assessed the applicability of three VIs in representing pan-Arctic vegetation carbon dynamics and then isolated the separate contributions of various climatic factors to terrestrial carbon dynamics variability from 2001 to 2023. The three VIs (NDVI, NIRv and kNDVI) showed increasing trends of 0.0005 ± 0.0008 yr^{-1}, 0.0017 ± 0.0014 yr^{-1} and 0.0009 ± 0.0013 yr^{-1} in the pan-Arctic ecosystems, accounting for 68.22 %, 74.49 % and 69.71 % of the total pan-Arctic grids, respectively. These greening trends in pan-Arctic terrestrial ecosystems may significantly affect the land–atmosphere energy balance and regional climate change. Both site-level and gridded validations revealed that the NIRv performed better than did the NDVI and kNDVI in representing pan-Arctic greening trends across plant functional types. Therefore, satellite-based NIRv data were used to indicate terrestrial carbon dynamics in pan-Arctic ecosystems. Further attribution analysis revealed that CO_2 and AT had positive partial correlations with satellite-

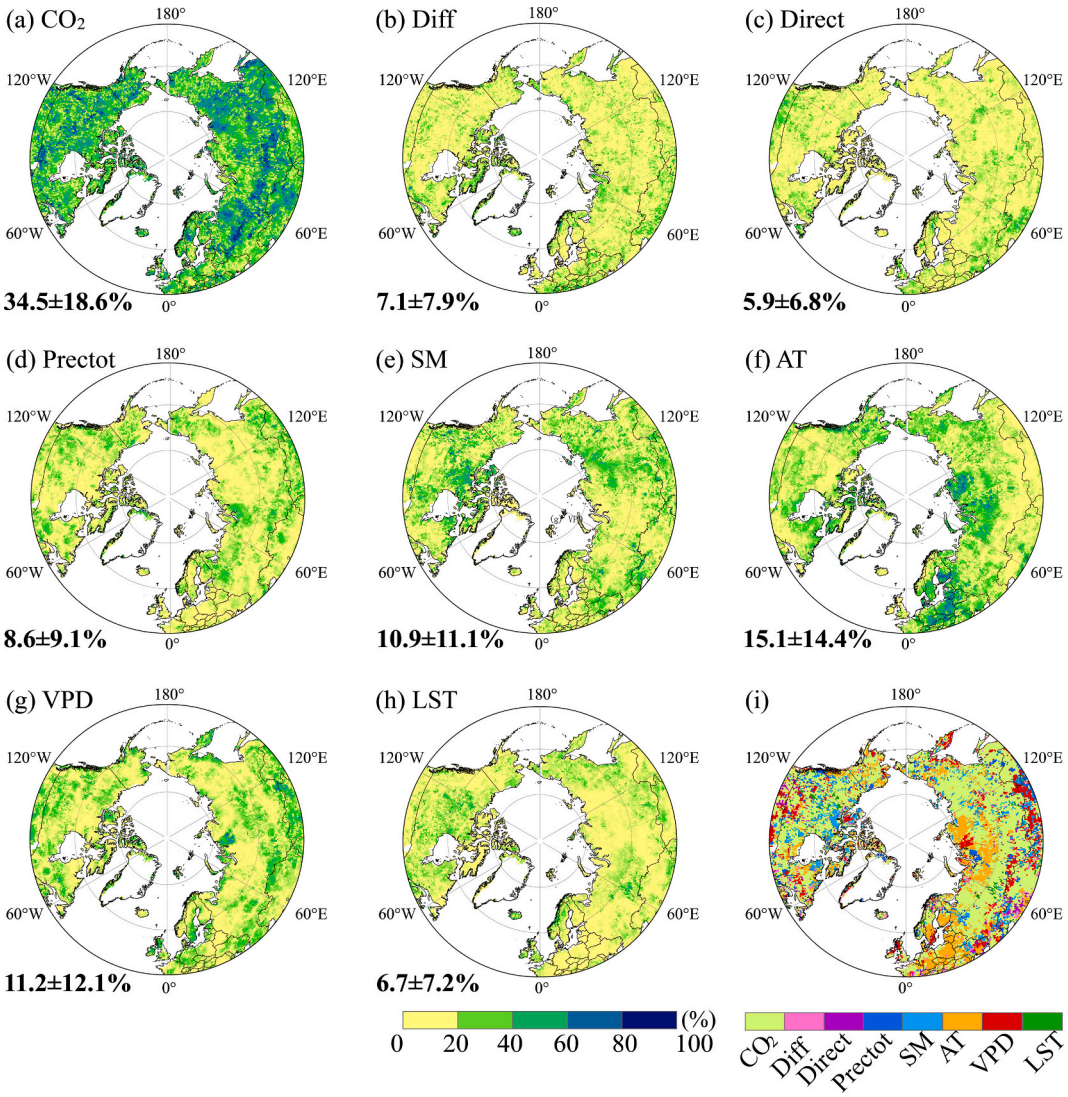

Fig. 8. The relative contributions of seven climatic factors to the NIRv in the pan-Arctic region from 2001 to 2023. Figure i illustrates the distribution of climatic factors with dominant contributions in different regions.

based NIRv measurements and contributed 34.5 % and 15.1 %, respectively, to carbon dynamics. In contrast, VPD showed positive (negative) partial correlations with NIRv variations in high (low) pan-Arctic ecosystems. Thus, VPD enhances carbon assimilation in the high-latitude pan-Arctic but weakens vegetation photosynthesis in the low-latitude pan-Arctic.

CRediT authorship contribution statement

Chengfeng Meng: Writing – original draft, Data curation. **Hao Zhou:** Writing – review & editing, Conceptualization. **Xichuan Liu:** Formal analysis, Data curation. **Jiao Zheng:** Methodology. **Jun Wang:** Writing – review & editing. **Qingwei Zeng:** Methodology. **Shuai Hu:** Methodology.

Declaration of competing interest

The authors declare no competing interests.

Acknowledgements

This research was jointly supported by National University of Defense Technology Youth Independent Innovation Science Fund project (grant no. ZK24-52), Hunan Science Fund for Distinguished Young Scholars (grant no. 2024JJ2058), and National Natural Science Foundation of China (grant no. 42175154, 62105367).

Appendix A. Supplementary data

Supplementary data to this article can be found online at https://doi.org/10.1016/j.ecoinf.2025.103267.

Data availability

The FLUXNET data are available at the website (https://fluxnet.org/data/fluxnet2015-dataset), and Gridded meteorological datasets are downloaded from https://gmao.gsfc.nasa.gov/reanalysis/MERRA-2/. GOSIF datasets can be downloaded through http://globalecology.unh.edu and CO_2 datasets can be downloaded from doi: https://doi.org/10.3974/geodb.2021.11.01.V1, and SM datasets can be downloaded from https://catalog.data.gov/dataset/ and MODIS reflectance data can be downloaded from https://lpdaac.usgs.gov/product_search/. Codes used in this study can be downloaded from https://zenodo.org/records/15597222.

References

Adams, H.D., Guardiola-Claramonte, M., Barron-Gafford, G.A., et al., 2009. Temperature sensitivity of drought-induced tree mortality portends increased regional die-off under global-change-type drought. Proc. Natl. Acad. Sci. USA 106, 7063–7066. https://doi.org/10.1073/pnas.0901438106.

Badgley, G., Field, C.B., Berry, J.A., 2017. Canopy near-infrared reflectance and terrestrial photosynthesis. Sci. Adv. 3, e1602244. https://doi.org/10.1126/sciadv.1602244.

Badgley, G., Anderegg, L.D.L., Berry, J.A., et al., 2019. Terrestrial gross primary production: using NIR $_V$ to scale from site to globe. Glob. Chang. Biol. 25, 3731–3740. https://doi.org/10.1111/gcb.14729.

Beer, C., Reichstein, M., Tomelleri, E., et al., 2010. Terrestrial gross carbon dioxide uptake: global distribution and covariation with climate. Science 329, 834–838. https://doi.org/10.1126/science.1184984.

Box, J.E., Colgan, W.T., Christensen, T.R., et al., 2019. Key indicators of Arctic climate change: 1971–2017. Environ. Res. Lett. 14, 045010. https://doi.org/10.1088/1748-9326/aafc1b.

Bruhwiler, L., Parmentier, F.-J.W., Crill, P., et al., 2021. The Arctic carbon cycle and its response to changing climate. Curr. Clim. Chang. Rep. 7, 14–34. https://doi.org/10.1007/s40641-020-00169-5.

Camps-Valls, G., Campos-Taberner, M., Moreno-Martínez, Á., et al., 2021. A unified vegetation index for quantifying the terrestrial biosphere. Sci. Adv. 无 7, eabc7447. https://doi.org/10.1126/sciadv.abc7447.

Chen, J.M., Cihlar, J., 1996. Retrieving leaf area index of boreal conifer forests using Landsat TM images. Remote Sens. Environ. 55, 153–162. https://doi.org/10.1016/0034-4257(95)00195-6.

Chen, X., Mo, X., Hu, S., et al., 2017. Contributions of climate change and human activities to ET and GPP trends over North China plain from 2000 to 2014. J. Geogr. Sci. 27, 661–680. https://doi.org/10.1007/s11442-017-1399-z.

Crichton, K.A., Anderson, K., Charman, D.J., et al., 2022. Seasonal climate drivers of peak NDVI in a series of Arctic peatlands. Sci. Total Environ. 838, 156419. https://doi.org/10.1016/j.scitotenv.2022.156419.

Durand, M., Murchie, E.H., Lindfors, A.V., et al., 2021. Diffuse solar radiation and canopy photosynthesis in a changing environment. Agric. For. Meteorol. 311, 108684. https://doi.org/10.1016/j.agrformet.2021.108684.

Erlandsson, R., Arneberg, M.K., Tømmervik, H., et al., 2023. Feasibility of active handheld NDVI sensors for monitoring lichen ground cover. Fungal Ecol. 63, 101233. https://doi.org/10.1016/j.funeco.2023.101233.

Gorelick, N., Hancher, M., Dixon, M., et al., 2017. Google earth engine: planetary-scale geospatial analysis for everyone. Remote Sens. Environ. 202, 18–27. https://doi.org/10.1016/j.rse.2017.06.031.

Green, J.K., Seneviratne, S.I., Berg, A.M., et al., 2019. Large influence of soil moisture on long-term terrestrial carbon uptake. Nature 565, 476–479. https://doi.org/10.1038/s41586-018-0848-x.

Heijmans, M.M.P.D., Magnússon, R.Í., Lara, M.J., et al., 2022. Tundra vegetation change and impacts on permafrost. Nat. Rev. Earth Environ. 3, 68–84. https://doi.org/10.1038/s43017-021-00233-0.

Hoerl, A.E., Kennard, R.W., 1970. Ridge regression: biased estimation for nonorthogonal problems. Technometrics 12, 55–67. https://doi.org/10.1080/00401706.1970.10488634.

Hollinger, D.Y., 1989. Canopy organization and foliage photosynthetic capacity in a broad-leaved Evergreen montane Forest. Funct. Ecol. 3, 53. https://doi.org/10.2307/2389675.

Hou, W., Jin, J., Jin, J., et al., 2021. Global Atmospheric Carbon Dioxide Concentration Simulation Grid Dataset (1992–2020). https://doi.org/10.3974/geodb.2021.11.01.V1.

Huete, A., Didan, K., Miura, T., et al., 2002. Overview of the radiometric and biophysical performance of the MODIS vegetation indices. Remote Sens. Environ. 83, 195–213. https://doi.org/10.1016/S0034-4257(02)00096-2.

Jiang, Z., Huete, A., Didan, K., et al., 2008. Development of a two-band enhanced vegetation index without a blue band. Remote Sens. Environ. 112, 3833–3845. https://doi.org/10.1016/j.rse.2008.06.006.

Jung, M., Koirala, S., Weber, U., et al., 2019. The FLUXCOM ensemble of global land-atmosphere energy fluxes. Sci. Data 6, 74. https://doi.org/10.1038/s41597-019-0076-8.

Konings, A.G., Williams, A.P., Gentine, P., 2017. Sensitivity of grassland productivity to aridity controlled by stomatal and xylem regulation. Nat. Geosci. 10, 284–288. https://doi.org/10.1038/ngeo2903.

Lemaire, G., Francois, C., Soudani, K., et al., 2008. Calibration and validation of hyperspectral indices for the estimation of broadleaved forest leaf chlorophyll content, leaf mass per area, leaf area index and leaf canopy biomass. Remote Sens. Environ. 112, 3846–3864. https://doi.org/10.1016/j.rse.2008.06.005.

Li, X., Xiao, J., 2019. A global, 0.05-degree product of solar-induced chlorophyll fluorescence derived from OCO-2, MODIS, and reanalysis data. Remote Sens. 11, 517. https://doi.org/10.3390/rs11050517.

Li, G., Wu, C., Chen, Y., et al., 2023. Increasing temperature regulates the advance of peak photosynthesis timing in the boreal ecosystem. Sci. Total Environ. 882, 163587. https://doi.org/10.1016/j.scitotenv.2023.163587.

Li, X., Huntingford, C., Wang, K., et al., 2024. Increased crossing of thermal stress thresholds of vegetation under global warming. Glob. Chang. Biol. 30, e17406. https://doi.org/10.1111/gcb.17406.

Li, X.L., Yang, X., Zhang, Z., Zhai, J.B., Meng, X.X., 2025. Evaluating of ground surface freeze–thaw and the interrelationship with vegetation cover on the Qinghai-Xizang plateau. Geoderma 453, 0016–7061. https://doi.org/10.1016/j.geoderma.2024.117141.

Liu, L., Gudmundsson, L., Hauser, M., et al., 2020. Soil moisture dominates dryness stress on ecosystem production globally. Nat. Commun. 11, 4892. https://doi.org/10.1038/s41467-020-18631-1.

Maes, S.L., Dietrich, J., Midolo, G., et al., 2024. Environmental drivers of increased ecosystem respiration in a warming tundra. Nature 629, 105–113. https://doi.org/10.1038/s41586-024-07274-7.

Myers-Smith, I.H., Kerby, J.T., Phoenix, G.K., et al., 2020. Complexity revealed in the greening of the Arctic. Nat. Clim. Chang. 10, 106–117. https://doi.org/10.1038/s41558-019-0688-1.

Nakatsubo, T., Hirota, M., Kishimoto-Mo, A.W., et al., 2023. Carbon exchange and primary production in a high-Arctic peatland in Svalbard. Polar Res. 42. https://doi.org/10.33265/polar.v42.8541.

Novick, K.A., Ficklin, D.L., Stoy, P.C., et al., 2016a. The increasing importance of atmospheric demand for ecosystem water and carbon fluxes. Nat. Clim. Chang. 6, 1023–1027. https://doi.org/10.1038/nclimate3114.

Novick, K.A., Miniat, C.F., Vose, J.M., 2016b. Drought limitations to leaf-level gas exchange: results from a model linking stomatal optimization and cohesion–tension theory. Plant Cell Environ. 39, 583–596. https://doi.org/10.1111/pce.12657.

Oehri, J., Schaepman-Strub, G., Kim, J.-S., et al., 2022. Vegetation type is an important predictor of the arctic summer land surface energy budget. Nat. Commun. 13, 6379. https://doi.org/10.1038/s41467-022-34049-3.

Park, T., Ganguly, S., Tømmervik, H., et al., 2016. Changes in growing season duration and productivity of northern vegetation inferred from long-term remote sensing data. Environ. Res. Lett. 11, 084001. https://doi.org/10.1088/1748-9326/11/8/084001.

Pastorello, G., Trotta, C., Canfora, E., et al., 2020. The FLUXNET2015 dataset and the ONEFlux processing pipeline for eddy covariance data. Sci. Data 7, 225. https://doi.org/10.1038/s41597-020-0534-3.

Pearson, R.G., 2013. Shifts in Arctic vegetation and associated feedbacks under climate change. Nat. Clim. Chang. 3. https://doi.org/10.1038/nclimate1858.

Piao, S., Sitch, S., Ciais, P., et al., 2013. Evaluation of terrestrial carbon cycle models for their response to climate variability and to CO $_2$ trends. Glob. Chang. Biol. 19, 2117–2132. https://doi.org/10.1111/gcb.12187.

Ryu, Y., Jiang, C., Kobayashi, H., et al., 2018. MODIS-derived global land products of shortwave radiation and diffuse and total photosynthetically active radiation at 5 km resolution from 2000. Remote Sens. Environ. 204, 812–825. https://doi.org/10.1016/j.rse.2017.09.021.

Schimel, D., Stephens, B.B., Fisher, J.B., 2015. Effect of increasing CO $_2$ on the terrestrial carbon cycle. Proc. Natl. Acad. Sci. USA 112, 436–441. https://doi.org/10.1073/pnas.1407302112.

Sellers, P.J., 1987. Canopy reflectance, photosynthesis, and transpiration, II. The role of biophysics in the linearity of their interdependence. Remote Sens. Environ. 21, 143–183. https://doi.org/10.1016/0034-4257(87)90051-4.

Sellers, P.J., Berry, J.A., Collatz, G.J., et al., 1992. Canopy reflectance, photosynthesis, and transpiration. III. A reanalysis using improved leaf models and a new canopy integration scheme. Remote Sens. Environ. 42, 187–216. https://doi.org/10.1016/0034-4257(92)90102-P.

Sellin, A., Alber, M., Keinänen, M., et al., 2017. Growth of northern deciduous trees under increasing atmospheric humidity: possible mechanisms behind the growth retardation. Reg. Environ. Chang. 17, 2135–2148. https://doi.org/10.1007/s10113-016-1042-z.

Siriwardana, A.N., Kume, A., 2025. Introducing the spectral characteristics index: a novel method for clustering solar radiation fluctuations from a plant- ecophysiological perspective. Eco. Inform. 85, 1574–9541. https://doi.org/10.1016/j.ecoinf.2024.102940.

Sulman, B.N., Roman, D.T., Yi, K., et al., 2016. High atmospheric demand for water can limit forest carbon uptake and transpiration as severely as dry soil. Geophys. Res. Lett. 43, 9686–9695. https://doi.org/10.1002/2016GL069416.

Thakur, M.P., Tilman, D., Purschke, O., et al., 2017. Climate warming promotes species diversity, but with greater taxonomic redundancy, in complex environments. Sci. Adv. 3, e1700866. https://doi.org/10.1126/sciadv.1700866.

Tomimatsu, H., Tang, Y., 2016. Effects of high CO2 levels on dynamic photosynthesis: carbon gain, mechanisms, and environmental interactions. J. Plant Res. 129, 365–377. https://doi.org/10.1007/s10265-016-0817-0.

Tramontana, G., Jung, M., Camps-Valls, G., et al., 2016. Predicting Carbon Dioxide and Energy Fluxes Across Global FLUXNET Sites with Regression Algorithms. https://doi.org/10.5194/bg-2015-661.

Tucker, C.J., 1979. Red and photographic infrared linear combinations for monitoring vegetation. Remote Sens. Environ. 8, 127–150. https://doi.org/10.1016/0034-4257(79)90013-0.

Wang, S., Zhang, Y., Ju, W., et al., 2020. Recent global decline of CO $_2$ fertilization effects on vegetation photosynthesis. Science 370, 1295–1300. https://doi.org/10.1126/science.abb7772.

Wang, Z., Wu, J., Li, M., et al., 2024. The variability in sensitivity of vegetation greenness to climate change across Eurasia. Ecol. Indic. 163, 112140. https://doi.org/10.1016/j.ecolind.2024.112140.

Woodruff, D.R., Meinzer, F.C., McCulloh, K.A., 2010. Height-related trends in stomatal sensitivity to leaf-to-air vapour pressure deficit in a tall conifer. J. Exp. Bot. 61, 203–210. https://doi.org/10.1093/jxb/erp291.

Wu, K., Hu, Z., Wang, X., et al., 2024. Widespread increase in sensitivity of vegetation growth to climate variability on the Tibetan plateau. Agric. For. Meteorol. 358, 110260. https://doi.org/10.1016/j.agrformet.2024.110260.

Xie, S., Mo, X., Hu, S., et al., 2020. Contributions of climate change, elevated atmospheric CO2 and human activities to ET and GPP trends in the three-north region of China. Agric. For. Meteorol. 295, 108183. https://doi.org/10.1016/j.agrformet.2020.108183.

Xue, W., Zhang, J., Deng, X., et al., 2024. Responses of vegetation photosynthetic processes to aerosol-induced direct radiative effect in China. Atmos. Environ. 329, 120557. https://doi.org/10.1016/j.atmosenv.2024.120557.

Yuan, W., Zheng, Y., Piao, S., et al., 2019. Increased atmospheric vapor pressure deficit reduces global vegetation growth. Sci. Adv. 5, eaax1396. https://doi.org/10.1126/sciadv.aax1396.

Yuxi, W., Li, P., Yuemin, Y., et al., 2024. Global vegetation-temperature sensitivity and its driving forces in the 21st century. Earth's Future 12, e2022EF003395. https://doi.org/10.1029/2022EF003395.

Zeng, Y., Hao, D., Badgley, G., et al., 2021. Estimating near-infrared reflectance of vegetation from hyperspectral data. Remote Sens. Environ. 267, 112723. https://doi.org/10.1016/j.rse.2021.112723.

Zhang, Y., Piao, S., Sun, Y., et al., 2022. Future reversal of warming-enhanced vegetation productivity in the northern hemisphere. Nat. Clim. Chang. 12, 581–586. https://doi.org/10.1038/s41558-022-01374-w.

Zhang, J., Feng, Y., Maestre, F.T., et al., 2023. Water availability creates global thresholds in multidimensional soil biodiversity and functions. Nat. Ecol. Evol. 7, 1002–1011. https://doi.org/10.1038/s41559-023-02071-3.

Zhang, Ze, Li, X.L., Melnikov, A., et al., 2024a. Variations and driving factors of annual frequency of ground surface freeze–thaw in China. Clim. Dyn. 62, 1145–1157. https://doi.org/10.1007/s00382-023-06952-y.

Zhang, Z.D., Yue, X., Zhou, H., et al., 2024b. Simulation of the ecosystem productivity responses to aerosol diffuse radiation fertilization effects over the Pan-Arctic during 2001–19. Adv. Atmos. Sci. 41, 84–96. https://doi.org/10.1007/s00376-023-2329-x.

Zhao, Q., Zhu, Z., Zeng, H., et al., 2022. Seasonal peak photosynthesis is hindered by late canopy development in northern ecosystems. Nat. Plants 8, 1484–1492. https://doi.org/10.1038/s41477-022-01278-9.

Zhao, Y., Chen, Y., Wu, C., et al., 2023. Exploring the contribution of environmental factors to evapotranspiration dynamics in the Three-River-source region, China. J. Hydrol. 626, 130222. https://doi.org/10.1016/j.jhydrol.2023.130222.

Zheng, Y., Zhao, W., Chen, A., et al., 2024. Vegetation canopy structure mediates the response of gross primary production to environmental drivers across multiple temporal scales. Sci. Total Environ. 917, 170439. https://doi.org/10.1016/j.scitotenv.2024.170439.

Zhong, R., Wang, P., Mao, G., et al., 2021. Spatiotemporal variation of enhanced vegetation index in the Amazon Basin and its response to climate change. Phys. Chem. Earth A/B/C 123, 103024. https://doi.org/10.1016/j.pce.2021.103024.

Zhong, Z., He, B., Wang, Y.-P., et al., 2023. Disentangling the effects of vapor pressure deficit on northern terrestrial vegetation productivity. Sci. Adv. 9, eadf3166. https://doi.org/10.1126/sciadv.adf3166.

Zhou, H., Yue, X., Wang, B., et al., 2023. Distinguishing the main climatic drivers to the variability of gross primary productivity at global FLUXNET sites. Environ. Res. Lett. 18, 124007. https://doi.org/10.1088/1748-9326/ad059c.